Numerical Simulation of Two Phase Flows

Meng-Sing Liou
NASA John H. Glenn Research Center at Lewis Field
Cleveland, OH 44135, USA
E-mail: Meng-Sing.Liou@grc.nasa.gov
Phone: (216) 433-5855

Abstract

Two phase flows can be found in broad situations in nature, biology, and industry devices and can involve diverse and complex mechanisms. While the physical models may be specific for certain situations, the mathematical formulation and numerical treatment for solving the governing equations can be general. Based on the continuum mechanics, we shall treat the fluid as a mixture consisting of two interacting phases (or materials) occupying the same region in space at any given moment. Hence, we will require information concerning each individual phase as needed in a single phase, but also the interactions between them. These interaction terms, however, pose additional numerical challenges because they are beyond the basis that we use to construct modern numerical schemes, namely the hyperbolicity of equations. Moreover, due to disparate differences in time scales, fluid compressibility and nonlinearity become acute, further complicating the numerical procedures. In this paper, we will show the ideas and procedure how the AUSM-family schemes are extended for solving two phase flows problems. Specifically, both phases are assumed in thermodynamic equilibrium, namely, the time scales involved in phase interactions are extremely short in comparison with those in fluid speeds and pressure fluctuations. Details of the numerical formulation and issues involved are discussed and the effectiveness of the method are demonstrated for several industrial examples.

1 Extension to Real Fluids and Flows with Equilibrium Phase Change

Prior efforts in the construction of AUSM-type algorithms have assumed that the fluid behaves as an ideal gas or a mixture thereof. This section details recent extensions of AUSM-type schemes that are valid for generalized state equations, which may describe single-phase liquid, gas, or supercritical fluid behavior of a given substance. Due to the dramatic differences in compressibility among fluids in the different states and possible large differences in the flow speed, the "preconditioned" forms of the flux-splitting methods are utilized in the extensions. A second thrust of this section is to provide an initial direction toward the development of extensions suitable for solving the general multiphase flow problem for arbitrary flow speeds and arbitrary levels of compressibility. This initial step starts with the development of an equilibrium model for liquid-vapor phase transitions using information extracted from a generalized state equation. The resulting equations are similar to the preconditioned, perfect-gas Euler system in structure and in mathematical character but may admit such multiphase flow features as cavitation zones and vapor-liquid condensation shocks.

1.1 Real Fluid State Description

1.1.1 Single Phase Formulation

The thermodynamic state of a single-phase real fluid is defined by the relations $p = p(\rho, T)$ and $h = h(\rho, T)$. In the present work, we utilize the Peng-Robinson equation of state [1], a cubic formulation similar to the Van der Waals equation but generally much more accurate in the liquid phase. The Peng-Robinson equation is given by

$$p = Z(\rho, T)\rho RT. \tag{1.1}$$

This is a preprint or reprint of a paper intended for presentation at a conference. Because changes may be made before formal publication, this is made available with the understanding that it will not be cited or reproduced without the permission of the author.

$$Z(\bar{\rho}, T) = \frac{1}{1-b\bar{\rho}} - \frac{a(T)}{RT}\frac{\bar{\rho}}{1+2b\bar{\rho}-(b\bar{\rho})^2} \tag{1.2}$$

where $\bar{\rho}$ is the molar density ρ/M_w, M_w is the molecular weight, and R is the universal gas constant. A simple rearrangement leads to an equivalent cubic expression for the compressibility factor Z

$$Z^3 - (1-B)Z^2 + (A-3B^2-2B)Z - (AB-B^2-B^3) = 0 \tag{1.3}$$

$$A = \frac{a(T)p}{R^2T^2} \tag{1.4}$$

$$B = \frac{bp}{RT} \tag{1.5}$$

Given the fluid pressure and temperature, this equation may be solved for the compressibility factor, and the fluid molar density may be then be determined by

$$\bar{\rho} = \frac{p}{ZRT} \tag{1.6}$$

The constant b is a function of critical-point fluid properties, while the function $a(T)$ is a function of critical point properties and the fluid temperature. The functional form for $a(T)$ can differ depending on the polarity of the molecule. The calculations presented herein (for carbon dioxide (CO_2) and octane) utilize expressions derived in [1] and given below:

$$a(T) = a(T_c)\alpha(T_r,\omega), \quad T_r = \frac{T}{T_c} \tag{1.7}$$

$$a(T_c) = 0.45724\frac{R^2T_c^2}{P_c} \tag{1.8}$$

$$\alpha(T_r,\omega) = (1+\kappa(1-\sqrt{T_r}))^2 \tag{1.9}$$

$$\begin{aligned}\kappa &= 0.37464 + 1.54226\omega \\ &\quad - 0.26992\omega^2\end{aligned} \tag{1.10}$$

$$b = 0.07780\frac{RT_c}{P_c} \tag{1.11}$$

The critical point constants T_c and P_c and the accentricity factor ω are tabulated below for CO_2 and octane.

fluid	T_c (K)	P_c (Pa)	ω
CO_2	302.2	73.75e5	0.225
octane	569.4	24.96e5	0.4

The expressions presented above are strictly valid for non-polar molecules. Polar molecules, such as water, require different forms for a and b to match experimental liquid-state density and vapor pressure data properly.

Typical isotherms for the Peng-Robinson equation are plotted in Fig. 1.1 on a pressure-density diagram. Clearly indicated is the vapor regime, where pressure varies nearly linearly with density, and the liquid regime, where large pressure changes are required to induce a density change. For a given pressure and temperature, the solution of (1.3) returns one or three values of the compressibility factor Z, the former corresponding to the single-phase region (either liquid or vapor) and the latter corresponding to the two-phase region, where vapor and liquid may exist simultaneously. The corresponding densities for a pressure within the two-phase region are shown as points A-C. A and C represent saturated vapor and liquid states, while B is physically meaningless. For a particular temperature, the "allowable" two-phase region is bounded by the pressure values at D and E, which are local extrema. The loci of these pressure values for temperatures between the triple and critical points define liquid and vapor spinodal curves.

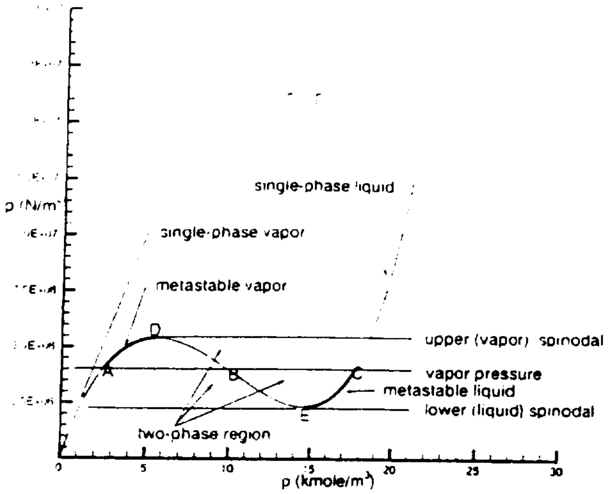

Figure 1.1: Pressure vs. molar density (isotherm below critical temperature).

dividing the two-phase region into metastable vapor, unstable, and metastable liquid regions. At a particular pressure between the liquid and vapor spinodal points, the system is in equilibrium, with the vapor and liquid fugacities attaining equal values. This pressure is known as the vapor pressure p_{vap} and is calculated as a function of temperature by iterating on the equation

$$f(Z_v,T,p) = f(Z_l,T,p), \tag{1.12}$$

where the fugacity f is given by

$$\ln\frac{f}{p} = Z - 1 - \ln(Z - B) - \frac{A}{2\sqrt{2}B}\ln\left(\frac{Z+(1+\sqrt{2})B}{Z+(1-\sqrt{2})B}\right). \tag{1.13}$$

The spinodal pressure and density values (points D and E in Fig. 1.1) can be obtained analytically by solving the quartic equation $\frac{\partial p}{\partial \rho}|_T = 0$, discarding two meaningless roots that occur outside the range of validity of the Peng-Robinson equation. The spinodal pressure values bound the actual vapor pressure, and an appropriate linear combination can be used as an initial guess for the iteration described above.

The thermodynamic state description for the single-phase fluid is completed by the specification of enthalpy departure functions [2], which introduce a density dependence into the enthalpy description and thus account for latent heat effects. For the Peng-Robinson equation, the enthalpy per unit mass of the fluid may be expressed as

$$h(\rho,T) = h_I(T) + \frac{1}{M_w}\left[RT(Z-1) + \frac{T\frac{da(T)}{dT} - a(T)}{2\sqrt{2}b}\ln\left(\frac{Z+(1+\sqrt{2})B}{Z+(1-\sqrt{2})B}\right)\right], \tag{1.14}$$

where $h_I(T)$ is the enthalpy per unit mass of an ideal gas at the same temperature (determined from curve fits presented in McBride, et al [3]).

The physical sound speed of the fluid can be calculated from thermodynamic considerations; a more useful CFD analogue is the acoustic eigenvalue, which may be obtained by determining the eigenvalues of the Jacobian matrix $\frac{\partial W}{\partial U}\frac{\partial F}{\partial W}$, where F is an Euler flux vector closed according to the general expressions $p = p(\rho,T)$ and $\rho h = \rho h(\rho,T)$. U is the vector of conserved variables, and W is the vector of primitive variables $[\rho,u,v,w,T]^T$. The choice of ρh (rather than h) and the choices of density and temperature as independent variables are dictated by the equilibrium description of the flow in the two-phase region is described later. For this choice of variables, the effective "sound speed" is given as

$$a^2 = \frac{(\rho h)_T p_\rho - p_T((\rho h)_\rho - h)}{(\rho h)_T - p_T} \tag{1.15}$$

1.1.2 Homogeneous Equilibrium Two-Phase Flow Model

The Peng-Robinson equation (and similar ones) gives no useful information in the unstable parts of the two-phase region. For densities between the spinodal values, it can be shown that the acoustic eigenvalues are complex, meaning that the Euler system is not hyperbolic in time and that conventional time-marching procedures for integrating the equations are ill posed. It is also of note that the liquid spinodal pressure may be negative for high molecular-weight liquids at lower temperatures, implying that the simulated expansion of a liquid might produce reasonable densities, but unphysical pressures, in the metastable region.

One means of avoiding these difficulties starts with the introduction of a void-fraction formalism for the two-phase region and the assumption of thermodynamic and kinematic equilibrium between the phases. For an equilibrium two-phase flow, the vapor pressure $p\text{vap}(T)$ is directly related to the temperature through the Clausius-Clapyron equation, and the density and temperature are independent variables. Given updated values for the density and temperature at a grid point as determined from a time-integration method, the following procedure is performed:

1. Determine the vapor pressure at that temperature, either through reference to a curve-fit or by the iterative procedure described above, and establish the saturation densities $\rho_l(T)$ and $\rho_v(T)$ and the saturation enthalpies $h_l(T)$ and $h_v(T)$ using (1.3), (1.6) , and (1.14).
2. If the fluid density is within the saturation limits, the equilibrium equation of state for the homogeneous mixture of liquid and vapor is given by

$$p = p\text{vap}(T) \tag{1.16}$$

$$\rho h(\rho, T) = \rho_v(T)\alpha_v(\rho, T)h_v(T) + \rho_l(T)\alpha_l(\rho, T)h_l(T) \tag{1.17}$$

$$\alpha_v(\rho, T) = \frac{\rho - \rho_l(T)}{\rho_v(T) - \rho_l(T)} \tag{1.18}$$

$$\alpha_l(\rho, T) = 1 - \alpha_v \tag{1.19}$$

3. If the density is not between the saturation values or the temperature is greater than the critical value, then the single phase description given by the Peng-Robinson equation will be used to determine the pressure and enthalpy.

In this description, the saturation-state values are strict functions of temperature; density dependence is introduced through the void fractions α and latent-heat effects arise through the change in departure enthalpy between the saturation states. The thermodynamic derivatives p_ρ, p_T, $(\rho h)_\rho$, and $(\rho h)_T$ needed in the time-integration method and in the sound speed definition can be computed by straightforward differentiation of the expressions above. These are discontinuous at phase transition points, leading to dramatic changes in the effective "sound speed" in the two-phase region. Figure 1.2 plots a^2 as a function of molar density for both the Peng-Robinson equation and the Peng-Robinson equation augmented by the equilibrium two-phase flow model (1.16-1.19). The fluid is octane at a temperature of 350 K. As shown, the equilibrium two-phase description preserves a real value for the "sound speed", while the basic Peng-Robinson equation results in negative values for a^2. Also shown is a theoretical result for the sound speed in a homogeneous two-phase mixture of liquid and vapor [4]:

$$\frac{1}{\rho a^2} = \frac{\alpha_v}{\rho_v a_v^2(T)} + \frac{\alpha_l}{\rho_l a_l^2(T)} \tag{1.20}$$

where $a^2_{v,l}(T)$ are obtained from (1.15) evaluated at the saturation states $\rho_{v,l}(T)$. The eigenvalue calculation for a^2 agrees reasonably well with the theoretical estimate except near single-phase

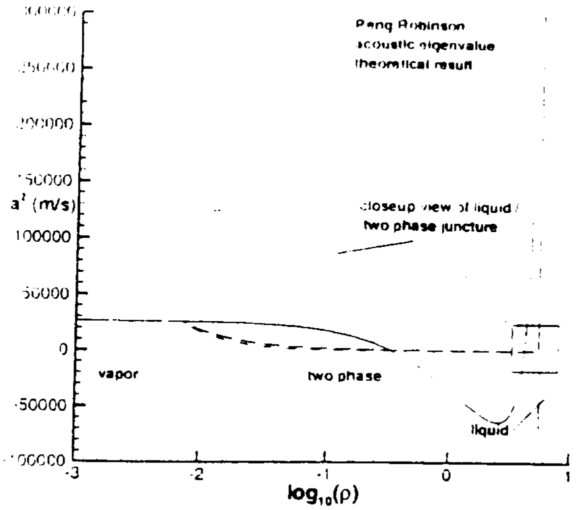

Figure 1.2: a^2 vs. molar density (octane at 350 K).

/ two-phase junctures, where the latter blends smoothly with the saturation-state values and the former exhibits a jump discontinuity. The theoretical expression for the sound speed is numerically more robust and is used in all calculations presented herein. Both expressions result in very small values (on the order of meters per second) for the "sound speed" near the liquid phase / two-phase interface, meaning that a shift to a locally "supersonic" flow condition during a phase transition is a distinct possibility.

The above formulation neglects velocity-slip effects, with the velocity actually solved for being a phase-weighted average velocity. This system is hyperbolic in character and is similar to the Euler system in structure but admits such multiphase features as cavitation zones and condensation shocks. A key element is the use of density and temperature as the "working" thermodynamic variables, particularly in contrast with the low-speed formulation described earlier, which utilizes pressure and temperature as the "working" thermodynamic variables. This choice is driven by the equilibrium closure for the two-phase region, in which pressure and temperature are not independent variables.

1.2 Time-Derivative Preconditioning

The utility of time-derivative preconditioning in the solution of the real fluid system described above lies in its ability to provide a smooth transition between nearly incompressible conditions (such as liquid phase or low Mach number vapor or supercritical fluid phase flows) and strongly compressible conditions (such as two-phase flows or high-speed vapor phase flows). As discussed previously, modifications to AUSM-type discretization are required to extend their range of applicability to flows at all speeds. These modifications depend on the choice of preconditioner, through the use of the eigenvalues of the preconditioned system. As in the previous work, the real fluid extension utilizes the preconditioner of Weiss and Smith [5], which may be expressed as a rank-one perturbation of the Jacobian matrix $\frac{\partial U}{\partial W}$. The time-derivative term in the real fluid Euler system is replaced by

$$\Gamma\frac{\partial W}{\partial t} \equiv \left(\frac{\partial U}{\partial W} + \Theta\vec{u}\vec{v}^T\right)\frac{\partial W}{\partial t} \tag{1.21}$$

where

$$\vec{u} = [1, u, v, w, H]^T \tag{1.22}$$

$$\vec{r} = [p, 0, 0, 0, pu]^T \qquad (1.23)$$

$$\Theta = \frac{1}{a^2 M_*^2} \qquad (1.24)$$

H is the total enthalpy per unit mass, and a is the acoustic speed defined earlier. The reference Mach number $M_*^2 \equiv \frac{V_*^2}{c^2}$ is given by

$$M_*^2 = \min(1, \max(M^2, M_{co}^2)) \qquad (1.25)$$

where M is the local Mach number (based on the velocity magnitude) and M_{co} is a user-specified cutoff Mach number discussed earlier. Again, the vector W is chosen as $[p, u, v, w, T]^T$ so that the proper closure of the system for an equilibrium two-phase flow is achieved. At low speeds, this preconditioner essentially replaces the physical thermodynamic derivative ρ_p with $1/V_*^2$, rescaling the eigenvalues of the Euler system so that the condition number remains bounded. This allows uniform convergence in both low-speed and high-speed flows. The eigenvalues of $\Gamma^{-1}A$ ($A = \partial F/\partial W$) are $u, u' \pm a'$, where u is the velocity component in the x direction and $u' \pm a'$ are as obtained in (??). Note that the real fluid state description does not affect the form of the eigenvalues - only the "sound speed" must be redefined.

1.3 AUSM-type Algorithms for Real Fluids

Procedures for extending AUSM-type algorithms to operate effectively in conjunction with time-derivative preconditioning have been proposed in [6]. These methods reduce to a standard upwind formulation at sonic transitions, preserving the discontinuity-capturing traits of the methods, but recover viable discretization of the incompressible flow equations as the Mach number approaches zero. As the real-fluid state description shares a structural similarity with the Euler system with and without preconditioning, it is anticipated that modifications to AUSM-type algorithms to allow accurate capturing of real fluid phenomena at all speeds should be relatively straightforward.

A key element in the construction of "all-speed" AUSM-type flux-splitting schemes is the need for including a pressure-diffusion term to couple the pressure and velocity fields at low Mach number. At higher speeds, the effect of the pressure-diffusion contribution is reduced (for AUSMDV and LDFSS) or eliminated (for AUSM+). For "preconditioned" AUSM+, the pressure-diffusion contribution to the interface flux can be written as

$$F_{1/2_{\text{pd, AUSM+}}} = \tilde{a}_{1/2}\left(\frac{1}{M_*^2} - 1\right)\mathcal{M}_{1/2_{\text{AUSM+}}} \times \frac{p_i - p_{i+1}}{\frac{p_i}{\rho_i} + \frac{p_{i+1}}{\rho_{i+1}}} \begin{bmatrix} 1 \\ u \\ v \\ w \\ H \end{bmatrix}_{i/i+1}, \qquad (1.26)$$

where $\tilde{a}$ is the "preconditioned" sound speed defined in (??) and evaluated using averages of left (i) and right ($i+1$ state information. The quantity $\mathcal{M}_{1/2_{\text{AUSM+}}}$ is an interface Mach number function, defined as

$$\mathcal{M}_{1/2_{\text{AUSM+}}} = \mathcal{M}^+_{(4,\beta)}(\bar{M}_i) - \mathcal{M}^+_{(1)}(\bar{M}_i) - \mathcal{M}^-_{(4,\beta)}(\bar{M}_{i+1}) + \mathcal{M}^-_{(1)}(\bar{M}_{i+1}) \qquad (1.27)$$

The subscript notation $i/i+1$ on the vector of "advected" variables $[1, u, v, w, H]^T$ indicates its evaluation at either the left or the right state, depending on the sign of the complete interface mass flux (advective contribution plus pressure diffusion contribution).[6] The "preconditioned" version of LDFSS [7] contains a similar term:

$$F_{1/2_{\text{pd, LDFSS}}} = \frac{\tilde{a}_{1/2}}{M_*^2}\mathcal{M}_{1/2_{\text{LDFSS}}} \times \frac{p_i - p_{i+1}}{p_i + p_{i+1}}\left[\rho_i \begin{bmatrix} 1 \\ u \\ v \\ w \\ H \end{bmatrix}_i + \rho_{i+1} \begin{bmatrix} 1 \\ u \\ v \\ w \\ H \end{bmatrix}_{i+1}\right]. \qquad (1.28)$$

where $\mathcal{M}_{1/2}$LDFSS is a different interface Mach number function

$$\mathcal{M}_{1/2}{}_{\text{LDFSS}} = \frac{1}{4}\left(\sqrt{\frac{1}{2}(M_i^2 + M_{i+1}^2)} - 1\right)^2 \tag{1.29}$$

In the limit of an incompressible flow, (ρ = constant, $a^2 \gg V^2$), the pressure-diffusion contribution to the mass flux for both schemes can be approximated as

$$\dot{m}_p \approx C_{1/2}\frac{\rho_{1/2}a_{1/2}^2}{p_{1/2}}\frac{\sqrt{a_{1/2}^2 + 4V_*^2}}{V_*^2}(p_i - p_{i+1}). \tag{1.30}$$

The function $C_{1/2}$ is scheme-dependent but is order unity. The coefficient $\frac{\rho_{1/2}a_{1/2}^2}{p_{1/2}}$ is also of order unity for gases, but for liquids and supercritical fluids governed by the Peng-Robinson equation, the coefficient may become much larger than unity. This represents an unphysical source of numerical diffusion for liquid-state calculations, one easily eliminated by redefining the pressure-diffusion contributions as

$$F_{1/2}{}_{\text{pd, AUSM+}} = \bar{a}_{1/2}\left(\frac{1}{M_*^2} - 1\right)\mathcal{M}_{1/2}{}_{\text{AUSM+}} \times \frac{p_i - p_{i+1}}{a_i^2 + a_{i+1}^2}\begin{bmatrix} 1 \\ u \\ v \\ w \\ H \end{bmatrix}_{i/i+1}, \tag{1.31}$$

and

$$F_{1/2}{}_{\text{pd, LDFSS}} = \frac{\bar{a}_{1/2}}{M_*^2}\mathcal{M}_{1/2}{}_{\text{LDFSS}} \times \frac{p_i - p_{i+1}}{\rho_i a_i^2 + \rho_{i+1}a_{i+1}^2}[\rho_i \begin{bmatrix} 1 \\ u \\ v \\ w \\ H \end{bmatrix}_i + \rho_{i+1}\begin{bmatrix} 1 \\ u \\ v \\ w \\ H \end{bmatrix}_{i+1}], \tag{1.32}$$

To enable an exact reduction to the appropriate incompressible limiting form, the interface sound speed can be redefined as

$$a_{1/2}{}_{\text{AUSM+}} = \sqrt{\frac{1}{2}(a_i^2 + a_{i+1}^2)} \tag{1.33}$$

and as

$$a_{1/2}{}_{\text{LDFSS}} = \sqrt{\frac{\rho_i a_i^2 + \rho_{i+1}a_{i+1}^2}{\rho_i + \rho_{i+1}}} \tag{1.34}$$

All other aspects of the flux-splitting are the same as outlined in Sections ?? and ?? and Refs. [6] and [7]. It should be noted that the modifications do affect the response of the schemes for perfect-gas calculations. For both schemes, the magnitude of the pressure diffusion contribution is lowered by a factor of $1/\gamma$, while for AUSM +, the ability of the scheme to capture a stationary shock wave with no intermediate point is disrupted by the definition in (1.33). Neither of these differences affects the performance of the schemes strongly.

1.4 Higher Order Extension

To extend the methods outlined above to second-order spatial accuracy, we utilize slope-limited Fromm interpolations of the primitive-variable vector $[\rho, u, v, w, T]^T$ to the $i + 1/2$ interface. As the state description is quite complex and expensive to calculate, some simplifications are employed. First, only the pressure and enthalpy are determined from the interpolated density and temperature. The much more expensive sound speed calculation is not performed as part of this interpolation, as the averages indicated in (1.31)-(1.34) are second order even if only nodal rather than interpolated data is used. A similar concession is made in the definition of the "preconditioned" sound speed (1.9), where again, only arithmetic averages using nodal quantities are used. As an example of this selective use of interpolated data, second order extensions of the AUSM+ and LDFSS pressure diffusion terms are shown below:

$$F_{1/2\,\mathrm{pd,\ AUSM+}} = \tilde{a}_{1/2}\left(\frac{1}{M_*^2} - 1\right)M_{1/2\,\mathrm{AUSM+}} \times \frac{p_L - p_R}{a_i^2 + a_{i+1}^2}\begin{bmatrix} 1 \\ u \\ v \\ w \\ H \end{bmatrix}_{L,R} \tag{1.35}$$

and

$$F_{1/2\,\mathrm{pd,\ LDFSS}} = \frac{\tilde{a}_{1/2}}{M_*^2}M_{1/2\,\mathrm{LDFSS}} \times \frac{p_L - p_R}{\rho_i a_i^2 + \rho_{i+1} a_{i+1}^2}[\rho_L \begin{bmatrix} 1 \\ u \\ v \\ w \\ H \end{bmatrix}_L + \rho_R \begin{bmatrix} 1 \\ u \\ v \\ w \\ H \end{bmatrix}_R], \tag{1.36}$$

In these, the notation L, R represents the use of interpolated values, whereas the notation $i, i+1$ represents the use of nodal values. Results shown later utilize both the minmod and Van Leer limiters in defining the interpolated data.

1.5 Applications

The techniques outlined in earlier sections have been incorporated into an implicit Navier-Stokes solver based on Gauss-Seidel relaxation [8], recently extended to multiblock domains. To minimize modifications to the code and to facilitate possible changes in the state description, the thermodynamic derivatives p_ρ, p_T, $(\rho h)_\rho$ and $(\rho h)_T$ are computed and stored as arrays, then used as needed in the construction of the flux Jacobian matrices. Viscosity and thermal conductivity data for the single-phase regions are taken from [9] and [10]. For the two-phase region, it is assumed that the mixture viscosity and thermal conductivity can be expressed as void-fraction weighted averages of the saturation-state values. A quasi- 1-D Euler solver has also been written to test basic attributes of the methods. The test cases below illustrate some general features of the schemes.

1.5.1 "Faucet" Problem

The "faucet" problem [11] is a classic test case for two-fluid codes. In the present context, the fluid is taken to be liquid octane in kinematic and thermodynamic equilibrium with its vapor at a temperature of 350 K and a vapor pressure of 2061 Pa. The calculation encompasses a one-dimensional domain of 12 m, with the inflow conditions specified by the temperature, the void fraction of octane vapor (taken as 0.2), and the velocity of the stream (taken as 10 m/s). The solution is forced by a gravity vector aligned in the direction of the flow, leading to acceleration of the fluid and an increase in the vapor-phase void fraction as the density decreases. A steady solution is obtained over time, with the transient response being the propagation of a discontinuous void wave downstream. With the present closure for the two-phase region, the problem is hyperbolic in the flow direction, as the effective "sound speed" is much smaller than the 10 m/s velocity. As such, all variables are fixed at the inflow and all are extrapolated at the outflow. Figure 1.3 presents calculation results for the void wave profile at a particular instance in time with an analytic solution for the two-phase, separated flow problem. A simple Euler explicit integration method is used. Only results from AUSM+ are shown, as both schemes revert to the same upwind-biased discretization for this problem. The first-order upwind scheme, operating at a CFL of 1.0, captures the void discontinuity rather sharply but diffuses the peak

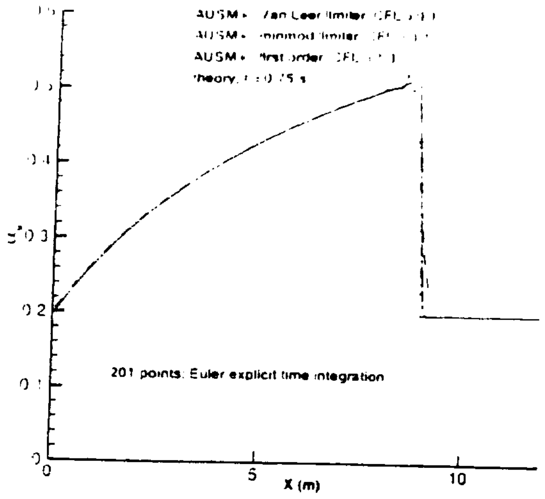

Figure 1.3: Octane vapor void fraction vs. x and time.

value. The second-order minmod and Van Leer - limited extensions require a much smaller CFL of 0.1 to maintain a reasonable degree of monotonicity in the void fraction profile. The Van Leer - limited case provides a slight improvement in the resolution of the peak value but due to the reduction in CFL number, the overall results are only marginally better than the first-order result. The minmod-limited result is slightly worse than the first-order result, again a consequence of the lower CFL number. It is likely that the second-order results would improve with the use of a more appropriate integration scheme.

1.5.2 Quasi - 1-D Liquid Expansion

The next test case considers the flow of initially liquid octane through a converging-diverging nozzle defined by the area relationship

$$A(x) = 1 + 4(x - 1/2)^2, 0 \leq x \leq 1 \tag{1.37}$$

The initial conditions are $p = 4 \times 10^7$ Pa, $T = 340$ K, and $u = 10$ m/s, with the nozzle exit pressure set to 0.7 times the initial pressure level. This problem mimics a cavitating flow in that the pressure drop experienced as the flow accelerates through the nozzle throat is steep enough to force a transition to the vapor phase. The fixed exit pressure forces a recompression back to the liquid state, simulating the collapse of a cavitation region. Figure 1.4 presents pressure distributions for three state equations: the Peng-Robinson (P-R) state description with the equilibrium two-phase flow model, an ideal gas equation of state, and the unmodified Peng-Robinson state description. As shown, the pressure level in the throat lowers to unphysical levels for the unmodified Peng-Robinson equation, representing a progression into the metastable liquid region. The equation system remains hyperbolic, however, as the density does not drop below the liquid spinodal value. In contrast, the pressure level for the Peng-Robinson equation with the equilibrium two-phase flow model lowers to the vapor pressure of octane. This results in the generation of a vapor phase and a decrease in the fluid density (Fig. 1.5). As expected, the liquid octane density varies little in the convergent section of the nozzle. The shock-like recompression of the two-phase fluid back to the liquid state is captured well by both the AUSM+ and LDFSS discretizations. Some effects of the higher-order extensions can be seen in the positioning of the condensation shock, and little difference between the AUSM+ and LDFSS predictions is observed. Pressure distributions from a perfect-gas closure are also shown in Fig.

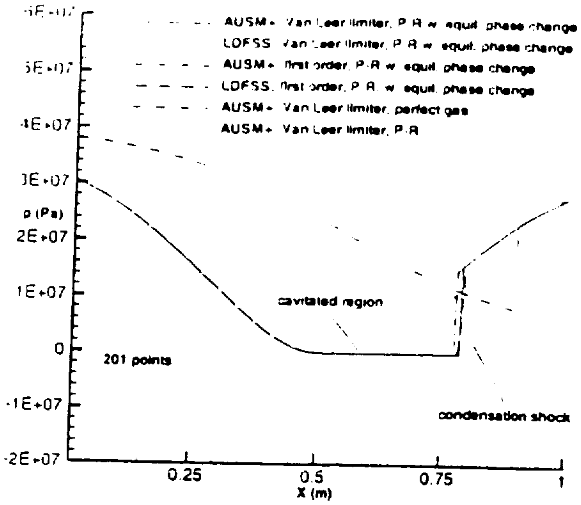

Figure 1.4: Pressure vs. x: expanding liquid octane.

1.4, with the comparisons highlighting the expected differences in the flow response due to the state description. The shock wave is captured monotonically by all methods.

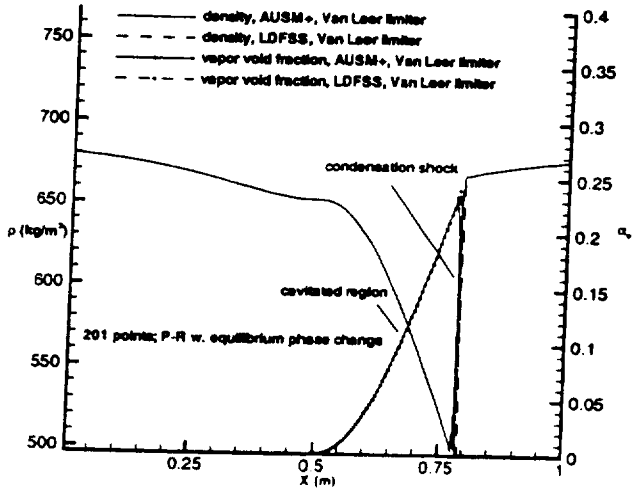

Figure 1.5: Density and vapor void fraction vs. x: expanding liquid octane.

1.5.3 Liquid CO_2 Expansion Through a Sharp Orifice Nozzle

Figure 1.6 illustrates axial velocity and density contours in the interior of a reservoir / capillary nozzle system for spraying liquid CO_2. A two-block grid is utilized, with the reservoir block containing 65x153 points and the capillary nozzle block containing 97x97 points. The flow is axisymmetric, and the reservoir total conditions are $p_o = 10 \times 10^6$ Pa and $T_o = 290K$. These conditions place the incoming fluid in the liquid state. The inflow boundary conditions fix the total pressure and temperature and extrapolate the v component of velocity from the interior. The expansion of the fluid around the sharp corner [illegible] enough to [illegible] the vapor phase, leading to a supersonic flow exiting the nozzle. The liquid / two-phase interface [illegible] with the sonic line and represents a discontinuity in the thermodynamic derivatives.

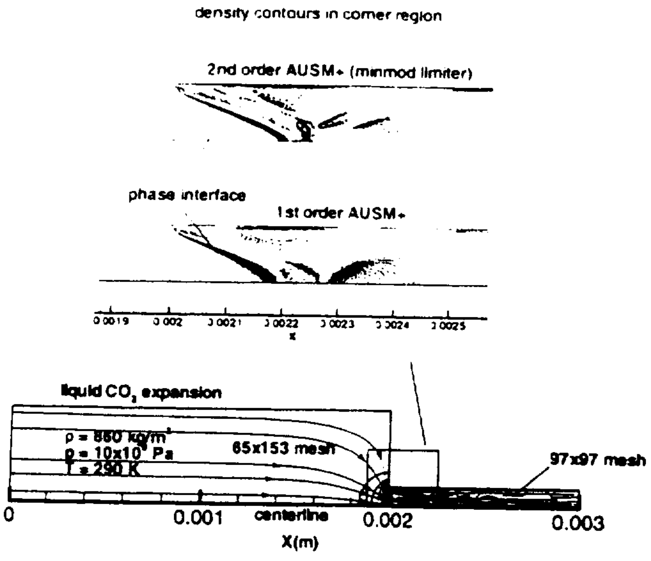

Figure 1.6: Velocity and density contours: liquid CO_2 expansion (AUSM+ upwinding).

No discontinuity in the bulk fluid properties is evidenced, however, as the transition into the two-phase region takes place very near the critical point of the fluid. Calculations without the equilibrium two-phase flow model were found to be unstable, as the rapid expansion drives the fluid density in the corner region below the liquid spinodal value. The pressure values remain reasonable, in contrast to the octane expansion described above, but the acoustic speeds become complex. Only AUSM+ solutions are shown; LDFSS solutions are very similar. The effects of the minmod-limited second-order extension are confined to the orifice region, where the second-order calculation results in more crisp predictions of the supersonic flow response. Features of note include regular oblique-shock and Mach wave reflections as well as a small pocket of reversed flow downstream of the corner. The displacement effect of this structure forms an area minimum, allowing the transition to supersonic flow.

1.5.4 Liquid Octane Expansion Through a Sharp Orifice Nozzle

The fourth test case involves the acceleration of liquid octane through a capillary tube. Devices similar to this are used in fuel injection systems. Again, a two-block grid is considered, with reservoir containing 65x153 nodes and the capillary tube containing 97x97 nodes. This problem is also axisymmetric, and the reservoir conditions are $p_o = 10 \times 10^6$ Pa and $T_o = 400K$. Octane is liquid under these conditions. The closeup in Fig. 1.7 plots density contours in the vicinity of the reservoir / tube juncture. The rapid pressure drop experienced as the fluid accelerates around the sharp corner cavitates the fluid, initially producing a bubble of nearly pure vapor. The wake of the bubble is a two-phase mixture of fluid, characterized by an increasing liquid content as the flow proceeds downstream. The two-phase / single-phase interface is sharply captured near the corner, with the shape of the bubble determined by a balance between the pressure jump and "numerical" surface tension resulting from the upwinding. Differences between first-order

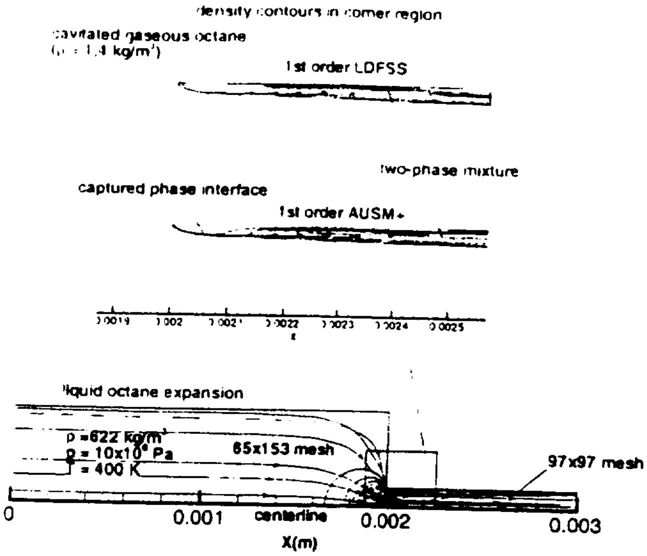
density contours in corner region
cavitated gaseous octane
(ρ = 1.4 kg/m^3)
1st order LDFSS
two-phase mixture
captured phase interface
1st order AUSM+
0.0019
0.002
0.0021
0.0022
0.0023
0.0024
0.0025
x
liquid octane expansion
ρ = 622 kg/m^3
p = 10x10^6 Pa
T = 400 K
65x153 mesh
97x97 mesh
0
0.001
centerline
0.002
0.003
X(m)

Figure 1.7: Density contours: octane cavitation.

AUSM+ and LDFSS solutions are minimal. These solutions are extremely difficult to obtain. With the current methods, the iteration must be nearly time-accurate with global time-stepping in order to capture stable bubble growth. Local time steps result in the intermittent appearance of octane vapor bubbles, which grow, propagate, and collapse in a highly unsteady manner. With the present thermodynamic model, the collapse of a vapor bubble results in higher temperatures, raising the vapor pressure and promoting more bubble growth. While many of these trends are consistent with the physics of cavitation bubble formation [4], the robustness and efficiency of the current procedures in capturing steady bubble behavior is a concern. The same is true for the higher-order extensions, which are even more susceptible to transient bubble growth. As a result, no higher-order solutions for this problem are yet available. Cavitation calculations using the Sanchez-Lacombe [12] equation of state, a lattice-fluid formulation valid for high molecular weight liquids, are underway for octane and water; these indicate somewhat better numerical behavior.

1.6 Concluding Remarks

Simple modifications for extending AUSM+ and LDFSS low-diffusion upwind schemes schemes toward the calculation of real fluids at all speeds and at all states of compressibility have been outlined in this section. The real fluid state description is based on the Peng-Robinson equation, enhanced by an equilibrium model for liquid-vapor phase transitions. Results indicate that the modifications proposed herein are effective in simulating incompressible liquid and compressible vapor responses as well as multiphase flow phenomena, such the appearance of cavitation bubbles and vapor-liquid condensation shocks. A point of concern is the robustness of the current procedures in capturing stationary cavitation bubbles - modifications to improve this behavior are underway. This work provides a starting point for a more comprehensive investigation of upwind discretization techniques for general nonequilibrium multiphase flows - efforts in this direction are also underway.

References

[1] Peng, D. Y. and Robinson, D. C., "A New Two-Constant Equation of State," *Ind. Eng. Chem. Fundam.*, Vol. 15, No. 1, 1976, pp. 59–64.

[2] Modell, M. and Reid, R. C., *Thermodynamics and Its Applications*, Prentice-Hall, Englewood Cliffs, New Jersey, 2nd ed.

[3] McBride, B. J., Gordon, S., and Reno, M. A., "Coefficients for Calculating Thermodynamic and Transport Properties of Individual Species," NASA TM TM-4513, October 1993.

[4] Brennen, C. E., *Cavitation and Bubble Dynamics, Oxford Engineering Science Series 44*, Oxford University Press, New York, 1995.

[5] Weiss, J. M. and Smith, W. A., "Preconditioning applied to variable and constant density time-accurate flows on unstructured meshes," AIAA Paper 94-2209, June 1994.

[6] Edwards, J. and Liou, M.-S., "Low-diffusion flux-splitting methods for flows at all speeds," *AIAA Journal*, Vol. 36, 1998, pp. 1610–1617.

[7] Edwards, J. R., "A low-diffusion flux-splitting scheme for Navier-Stokes calculations," *Computers & Fluids*, Vol. 26, 1997, pp. 635–659.

[8] Edwards, J. R. and Roy, C. J., "Preconditioned multigrid methods for two-dimensional combustion calculations at all speeds," *AIAA Journal*, Vol. 36, 1998, pp. 185–192.

[9] Olchowny, G. A. and Sengers, J. V., "Crossover from Singular to Regular Behavior of the Transport Properties of Fluids in the Critical Region," *Physical Review Letters*, Vol. 61, No. 1, pp. 15–18.

[10] Lee, H. and Thodos, G., "Generalized Viscosity Behavior of Fluids over the Complete Gaseous and Liquid States," *Ind. Eng. Chem. Res.*, Vol. 29, 1990, pp. 1404–1412.

[11] Ransom, V. H., "Numerical Benchmark Tests," *Multiphase Science and Technology, Vol. 3*, edited by G. F. Hewitt, J. M. Delhay, and N. Zuber, Hemisphere Publishing, Washington, DC, 1987.

[12] Sanchez, I. C. and Lacombe, R. H., "An Elementary Molecular Theory of Classical Fluids. Pure Fluids," *The Journal of Physical Chemistry*, Vol. 80, No. 21, 1976.